MSc in Photonics

PHOTONICS**BCN**

Universitat Politècnica de Catalunya (UPC)
Universitat Autònoma de Barcelona (UAB)
Universitat de Barcelona (UB)
Institut de Ciències Fotòniques (ICFO)

http://www.photonicsbcn.eu

Master in Photonics

MASTER THESIS WORK

Dynamics of a Bose Einstein condensate in a ring potential

Hernán Pino Quintana

Supervised by Dr. Verònica Ahufinger and Dr. Jordi Mompart, (UAB)

Presented on date 4th September 2012

Registered at

Escola Tècnica Superior d'Enginyeria de Telecomunicació de Barcelona

Dynamics of a Bose Einstein condensate in a ring potential

Hernán Pino Quintana.
Grup d' Òptica, Dept. de Física, Universitat Autònoma de Barcelona, E-08193 Bellaterra, Spain.

E-mail: enlil_kronos@hotmail.com

Abstract. We have addressed the dynamics of a repulsive interacting ^{87}Rb Bose Einstein condensate (BEC) in a ring potential trap. Our study has been focused in the analysis of the interference pattern that arises by the BEC self-interaction after its clockwise and counter-clockwise components overlap. We have numerically investigated the interference pattern obtained after the free expansion as well as the case for which an initial instantaneous transfer of momentum is provided to the BEC. The fringe spatial period has been numerically evaluated for different non-linear coupling values and compared with the classical prediction. Also, the velocity gradient has been calculated for the non-linear regime.

Keywords: Bose-Einstein condensation, atom optics

1. Introduction

Since the first experimental observation of Bose-Einstein condensation (BEC) in 1995 [1-3] the control of its coherent dynamics has become a subject of increasing interest. In this context, magnetic [4] and optical [5] trapping techniques for neutral atoms have been developed yielding a wide range of potential geometries such as single traps [5], straight and curved waveguides [6], periodic structures [7], and ring traps [8,9,10,11,12]. Among all these possible geometries, annular or ring traps are specially interesting since they present periodic boundary conditions and, therefore, become an ideal physical system to study quantum phase transitions [13], persistent currents [9,14,15], superconducting quantum interference devices (SQUID) [16], matter wave rotational sensors [17], control of cold collisions, solitons and vortices [18], and the observation of many-body physics [19]. Here we will consider trapping based only on optical means which is due to the dipole force of the light arising from the dispersive interaction of the induced atomic dipole moment with the intensity gradient of the light field [5]. Specifically, optical ring potentials have been experimentally implemented using time-averaged light fields [8], Laguerre-Gauss beams [9,10,11] and conical refraction [12].

In this work, we will investigate the dynamics of a repulsive interacting BEC loaded in a ring trap from a symmetric harmonic potential by means of the two-dimensional (2D) Gross-Pitaevskii equation (GPE). We will perform numerical simulations by integrating the 2D GPE with the Crack-Nicholson technique. In particular, we will address three different cases: (i) the free expansion of the BEC along the ring; (ii) the motion after an instantaneous transfer of momentum in one direction, and (iii) the splitting of the BEC in two components counter propagating along the ring. In the three cases, we will analyze the interference pattern that arises when the BEC, propagating clock wise and counter-clock wise along the ring, overlaps with itself. In Section 2, we describe the physical system under consideration while Section 3 is devoted to briefly discuss the physical origin of the interferences. The free evolution of the BEC along the ring is discussed in Section 4, and its dynamics after the instantaneous transfer of momentum is studied in Section 5. Section 6 summarizes the work and presents the conclusions.

2. Physical system

We will consider a physical system consisting of a repulsive interacting BEC of ^{87}Rb loaded in a ring trap which, at zero temperature and in the mean field approximation, is described by the GPE [20]:

$$i\hbar\frac{\partial}{\partial t}[\psi(\boldsymbol{r},t)] = \left(-\frac{\hbar^2}{2m}\nabla^2 + V_{ext}(\boldsymbol{r},t) + g|\psi(\boldsymbol{r},t)|^2\right)\psi(\boldsymbol{r},t), \quad (1)$$

where $\hbar$ is the reduced Planck's constant and m is the mass of the atoms that form the BEC.

The first term in the right hand side of equation (1) is associated with the kinetic energy. The second term describes the external trapping potential that we take:

$$V_{ext} = \frac{1}{2}m{\omega_r}^2(\rho-\rho_0)^2 + \frac{1}{2}m{\omega_\perp}^2 z^2, \quad (2)$$

with $\rho^2 = x^2 + y^2$. The trapping potential (2) consists of two contributions: the first one is a ring with mean radius ρ_0 whose harmonic radial profile has a frequency ω_r, and the second one is a tight harmonic trap in the z direction with frequency $\omega_\perp$. Finally, the last term of the right hand side of (1) is the nonlinear contribution associated to the atom-atom interaction within the BEC where the coupling constant g is defined as [20]:

$$g = \frac{4\pi\hbar^2 a_s N}{m}, \quad (3)$$

being a_s the scattering length and N the total number of particles. Along this work, we will consider values for ^{87}Rb atoms, i.e., $a_s = 5.8\cdot 10^{-3}$ μm, $m = 1.45\cdot 10^{-25}$ Kg and different values of N.

By imposing that the transverse trapping potential is much tighter than the radial one i.e., $\omega_\perp \gg \omega_r$, the dynamics can be restricted to two dimensions in the so-called "pancake" geometry. In this situation, one can factorize the wave function as $\psi(\boldsymbol{r},t) = \eta(z)\varphi(x,y,t)$, where $\eta(z)$ is the solution for the ground state of the transverse harmonic potential. Then, integrating equation (1) over the z dimension, one obtains the 2D GPE:

$$i\hbar\frac{\partial}{\partial t}[\varphi(x,y,t)] = \left(-\frac{\hbar^2}{2m}\nabla^2 + V_{2D} + g_{2D}|\varphi(x,y,t)|^2\right)\varphi(x,y,t), \quad (4)$$

where the Laplacian only applies to the x and y coordinates, and the external potential reads:

$$V_{2D} = \frac{1}{2}m{\omega_r}^2(\rho-\rho_0)^2. \quad (5)$$

To illustrate the trapping geometry that we will use in the numerical simulations of Sections 4 and 5, Figure 1 shows the width of the radial harmonic ring potential, characterized by 3α where $\alpha = \sqrt{\hbar/m\omega_r}$, for $\rho_0 = 8$ μm and $\omega_r = 2\pi\times 1$ KHz.

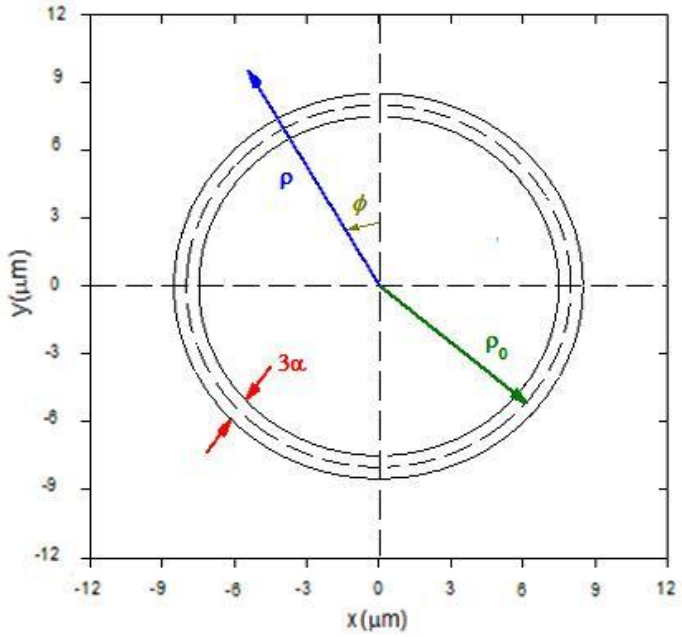

Figure 1. Sketch of the 2D ring trapping potential for $\rho_0 = 8\ \mu$m, $\omega_r = 2\pi \times 1$ KHz and $m = 1.45 \cdot 10^{-25}$ Kg. For an easy visualization of the ring, its width in the figure is characterized by 3α where $\alpha = \sqrt{\hbar/m\omega_r}$ is the ground state width for the radial harmonic potential.

In 2D, the non-linear coupling constant is re-defined as [20]:

$$g_{2D} = a_s N \sqrt{\frac{8\pi\omega_\perp \hbar^3}{m}}. \tag{6}$$

In this work, we are interested in the dynamics of a ^{87}Rb BEC loaded in the ring potential described above. The loading is performed from a symmetric harmonic potential as it is usually done in the experiments [6]. Therefore, we start first by looking for the ground state of (4) by means of the Crank-Nicholson method in imaginary time with the following isotropic harmonic potential:

$$V_h = \frac{1}{2} m {\omega_h}^2 (x^2 + y^2). \tag{7}$$

In order to avoid radial excitations during the loading process, ω_h should match the radial trapping frequency of the ring ω_r keeping the transverse confinement tight enough to ensure that the dynamics is two dimensional. Figure 2 shows the density profile of the obtained ground state for $\omega_h = \omega_r = 2\pi \times 1$ KHz and $\omega_\perp = 5\ \omega_h$ presenting the characteristic parabolic-type profile of a repulsive BEC. To study the dynamics of the BEC along the ring (see Sections 4 and 5), we will always proceed by calculating first the initial state as has been indicated in the previous lines.

3. Interference pattern

Once the BEC is loaded into the ring, it will propagate both clockwise and counter-clockwise along the ring to eventually self-interact in the overlapping region. To characterize the interference pattern, we assume, as a first approximation, that the BEC wavefunction in the interference region can be described as two counterpropagating plane waves:

$$\varphi = |\varphi^{\circlearrowleft}| e^{+ikx} + |\varphi^{\circlearrowright}| e^{-ikx}, \tag{8}$$

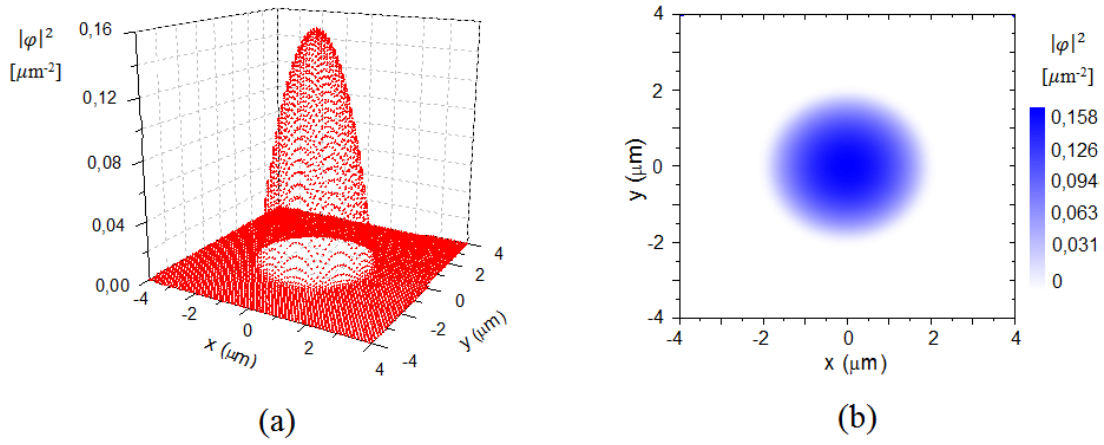

Figure 2. Ground state density profile of a ^{87}Rb BEC of 5000 atoms in a 2D harmonic trap with $\omega_h = 2\pi \times 1$ KHz and $\omega_\perp = 5\,\omega_h$. (a) XYZ plot and (b) density plot.

where k is the wavenumber of each component. Assuming the fully symmetric case given by $|\varphi^{\circlearrowleft}| = |\varphi^{\circlearrowright}|$, the density distribution at the interference region will be proportional to:

$$|\varphi|^2 \propto \cos^2 kx, \tag{9}$$

which gives a fringe spatial period $\Delta x = \pi/k$. On the other hand, the wavenumber is related to the atomic velocity by de Broglie's relation:

$$k = \frac{mv}{\hbar}. \tag{10}$$

For a non-interacting BEC the velocity in the interference region can be estimated to be $v = \pi\rho_0/t_{int}$, being ρ_0 the mean radius of the ring potential, and t_{int} the time at which interferences are observed (t = 0 corresponds to the time at which the BEC loading takes place). Combining (9), (10) and the velocity estimation, one obtains the following expression for the fringe spatial period:

$$\Delta x = \frac{\hbar t_{int}}{m\rho_0}. \tag{11}$$

This expression is in full agreement with the one derived in Ref. [21] where two condensates separated a linear distance d overlap after free expansion where the nonlinear interactions become negligible. Note that expression (11) has been derived assuming two point-like BECs, does not account for the role of the non-linearity in the fringe spatial period, and, therefore, should be considered as a classical approximation.

In our case, after the BEC is loaded into the ring, it expands mainly due to the conversion of the mean-field energy into kinetic energy [6]. Since the mean-field energy is proportional to the parabolic density distribution, the BEC acquires a velocity field that linearly increases with the position $v(\phi, t) = \beta(t)\rho_0\phi$ where $\beta(t)$ is the velocity gradient of the BEC. Thus, the fringe spatial period measured at the interference region can be used to deduce:

$$\beta(t) = \frac{\hbar}{m\rho_0\Delta x}. \tag{12}$$

Sections 4 and 5 will be devoted to the numerical simulation of the BEC dynamics along the ring by integrating the corresponding GPE with the Crack-Nicholson method and for different initial conditions. In all cases, we will investigate the interference pattern and compare the numerical results for the fringe spatial period with expressions (11) and (12).

4. Interferences after free expansion

The first case that we consider is the free expansion of the ^{87}Rb BEC (N = 5000) after its loading into the ring trap potential at $\phi = 0$ with $\rho_0 = 8\ \mu$m and $\omega_r = 2\pi \times 1$ KHz. We will study the corresponding interference pattern generated by their self-interaction in the ring at $\phi = \pi$. The state that we load in the ring corresponds to the ground state of the 2D harmonic potential calculated as described in Section 2 with $\omega_r = \omega_h$. Figure 3 shows the dynamics of the BEC from $t = 0$ ms to $t = 2$ ms and the interference pattern at $t = 2$ ms.

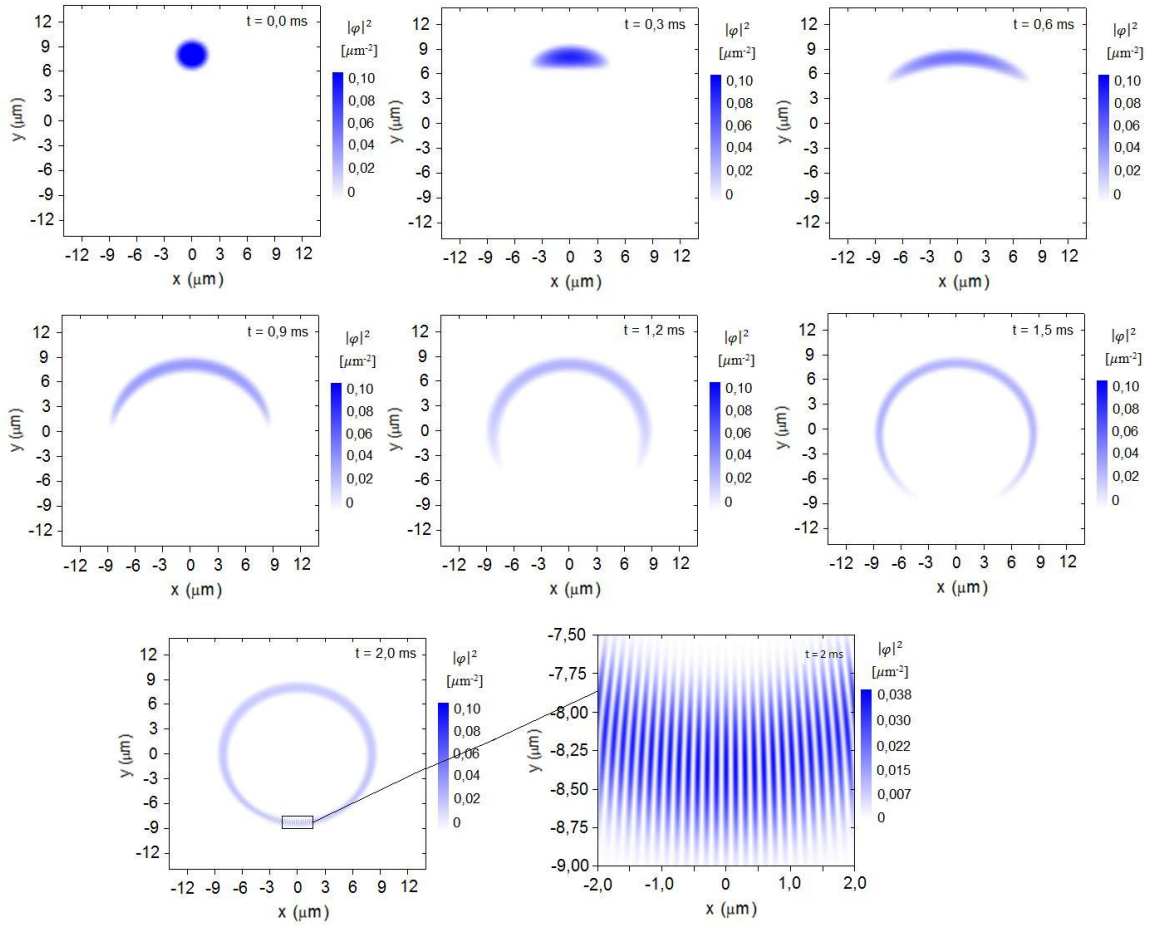

Figure 3. Density plot of the temporal evolution of the density distribution for a ^{87}Rb BEC of 5000 atoms during its free expansion along a ring potential with $\rho_0 = 8\ \mu$m, $\omega_r = 2\pi \times 1$ KHz, and $\omega_\perp = 5\ \omega_r$. The last picture shows an enlarged view of the interference region at $t = 2$ ms.

The observed fringe spatial period in Figure 3 is $\Delta x_{\text{obs}}(t_{int} = 2\text{ ms}) = 0.146\ \mu$m that is close to the predicted one obtained from expression (11) that yields $\Delta x(t_{int} = 2\text{ ms}) = 0.181\ \mu$m. This difference is mainly due to the fact that the non-linearity has not been included in the derivation of expression (11). To analyze the role of the non-linearity in the fringe spatial period we have simulated the free expansion of the BEC for different number of atoms (alternatively, it could be possible to do it by modifying the value of scattering length, under for instance, a Feshbach resonance). Figure 4 shows the fringe spatial period as a function of time for different values of the non-linear coupling g_{2D} obtained varying the number of atoms. It is clearly seen

in the first row of this figure that as the number of atoms decreases and, therefore, the coupling g_{2D} also decreases, the fringe spatial period behavior gets closer to the classical prediction (11), i.e., it exhibits a linear dependence with nearly the same slope as (11). Note also that as being the non-linearity repulsive, it leads to a faster free expansion of the BEC for higher values of the non-linearity. This, in turn, increases the BEC velocity and, therefore, reduces the time for which the interferences start to appear.

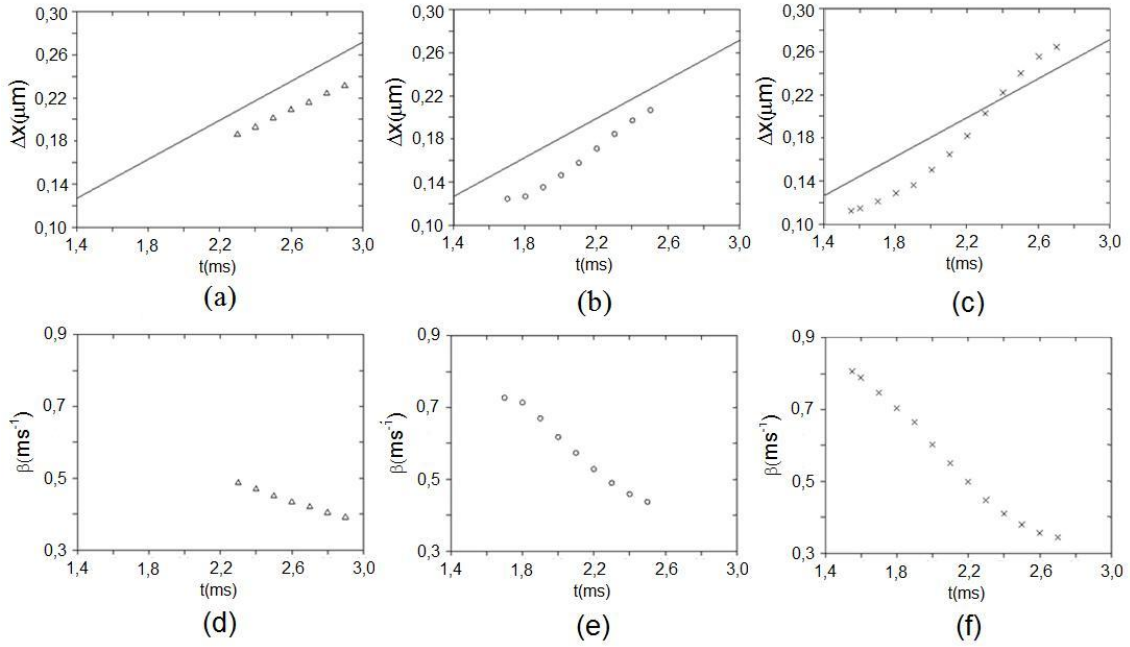

Figure 4. Time evolution of the fringe spatial period for (a) $N = 1000$ (triangles), (b) $N = 5000$ (circles), (c) $N = 10000$ (crosses). The solid line in (a), (b) and (c) corresponds to the relation (11) with $\rho_0 = 8\,\mu$m and $m = 1.45 \cdot 10^{-25}$ Kg. The time evolution of the velocity gradient β (12) is plotted in the second row for (d) $N = 1000$ (triangles), (e) $N = 5000$ (circles) and (f) $N = 10000$ (crosses). The rest of parameters are the same as in Figure 3.

For large number of atoms, the classical approximation does not accurately describe the numerically obtained behaviour and the nonlinear expression (12) for the fringe spatial period should be used. In the bottom row of Figure 4 we represent the time-dependent velocity gradient in the interference region, associated to the corresponding numerical simulation, showing how the difference between the BEC velocity propagation for different wave fronts becomes higher as the non-linearity increases in contrast with the expected behaviour when the non-linear contribution becomes smaller.

To characterize the dynamics of the BEC in the ring, we have defined the following parameter $R = \sqrt{< x >^2 + < y >^2}$ (where $< x >$ and $< y >$ are the x and y mean positions for the BEC wavefunction with respect to the center of the ring). This parameter indicates the degree of localization of the BEC. Figure 5 illustrates the temporal evolution of R for different values of the number of particles during the BEC expansion. In all cases, the BEC, created in a 2D isotropic harmonic potential with frequencies identical to the radial one of the ring, is loaded at $\phi = 0$, and, therefore, the initial value of R coincides with $\rho_0 = 8\,\mu$m. As the BEC spreads along the ring, the value of R decreases and interferences at $\phi = \pi$ start to appear. When the BEC completely fills homogeneously the ring, then R=0. As the non-linear contribution increases, the free expansion of the condensate is faster leading to a higher slope in Figure 5. Note that for the extreme case in which the non-linearity is turned off, the expansion of the condensate is a few orders of magnitude slower than for the case of N = 10000 atoms.

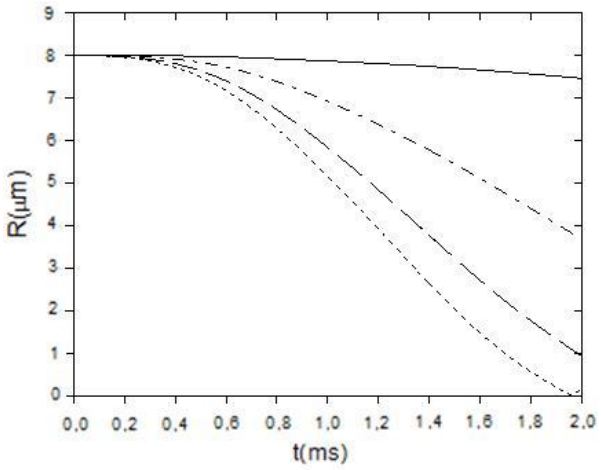

Figure 5. Plot of the temporal evolution of the parameter $R = \sqrt{< x >^2 + < y >^2}$ during the free expansion of a ^{87}Rb condensate for $N = 1000$ (dashed dot line), $N = 5000$ (dashed line) and $N = 10000$ (dotted line). The solid line corresponds to $g_{2D} = 0$. The rest of parameters are the same as in Figure 3.

5. Interferences after initial momentum transfer

In the following section, we study the dynamics of the BEC after providing an initial instantaneous transfer of momentum by imposing a linear phase spatial dependence to the condensate wavefunction. This transfer of momentum is numerically implemented by multiplying the wavefunction by $exp(-ikx)$. It is important to consider that the energy added to the system should be low enough in order to avoid excitations in the radial direction. Thus, the value of the initial momentum is bounded from above. The upper bound is obtained when the kinetic energy $E_k = \frac{(k\hbar)^2}{2m}$ is equal to the energy difference between the ground and the first excited state in the radial harmonic potential, $\Delta E_h = \hbar\omega_r$, giving:

$$k_{max} = \sqrt{\frac{2m\omega_r}{\hbar}}. \tag{13}$$

For the parameters that we have used in Figs. 2 and 3, one obtains from (13) that $k_{max} = 4.17\ \mu\text{m}^{-1}$.

5.1. Single momentum transfer

Figure 6 shows the dynamics of the condensate after an initial transfer of momentum of $k = 4\ \mu\text{m}^{-1}$ in the direction *x*. Due to the asymmetric transfer of momentum the clock an counter-clock wise components have different amplitudes and velocities. Therefore, the interference region arises at $\phi > \pi$. The observed fringe spatial period for $t = 2$ ms is $\Delta x_{\text{k,obs}}(t_{int} = 2\text{ ms}) = 0.144\mu\text{m}$, value that nearly coincides with the observed in Figure 3, $\Delta x_{\text{obs}}(t_{int} = 2\text{ ms}) = 0.146\ \mu\text{m}$. This coincidence is surprising since in the present case we are far away from the conditions of validity of expression (11). In particular, the completely symmetric splitting assumed in equation (8)-(9) is not fulfilled now.

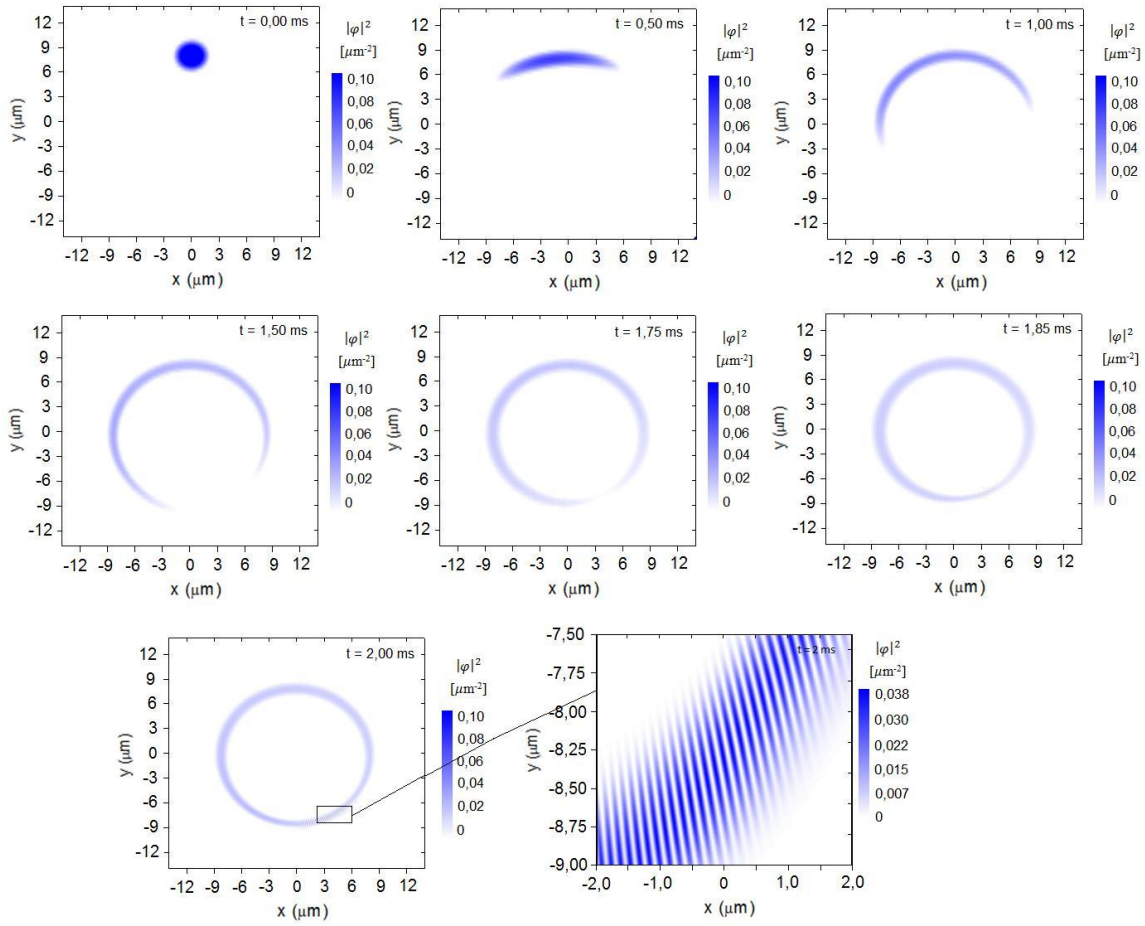

Figure 6. Density plot of the temporal evolution of the density distribution for a ^{87}Rb BEC of 5000 atoms in a ring potential with $\rho_0 = 8\ \mu$m, $\omega_r = 2\pi \times 1$ KHz, and $\omega_\perp = 5\ \omega_r$, after an initial transfer of momentum of $k = 4\ \mu$m^{-1} in the x direction. Last picture shows an enlarged view of the interference region at $t = 2$ ms. The rest of parameters are the same as in Figure 3.

5.1. Double momentum transfer

Now, we will apply an initial symmetric transfer of momentum along $\pm x$ of $k = 4\ \mu$m^{-1} to the ^{87}Rb BEC loaded in the ring. In this case, the symmetry of the dynamics is kept allowing to study the influence of the external momentum in the fringe spatial period following the lines of equations (8)-(12). In Figure 7, we have plotted the time evolution of the density distribution. The observed fringe spatial period now, $\Delta x_{\pm \mathrm{k,obs}}(t_{int} = 2\ \mathrm{ms}) = 0.158\ \mu$m, is larger than the $0.146\ \mu$m value observed for free expansion. We plot in Figure 8 the time dependence of the fringe spatial period and the associated velocity gradient $\beta(t)$ calculated with expression (12). We see, as expected, how the addition of the transfer of momentum induces an increase of the propagation velocity along the ring which according to expressions (9)-(11) implies a higher value of the spatial fringe period although the slope of the both cases remains similar.

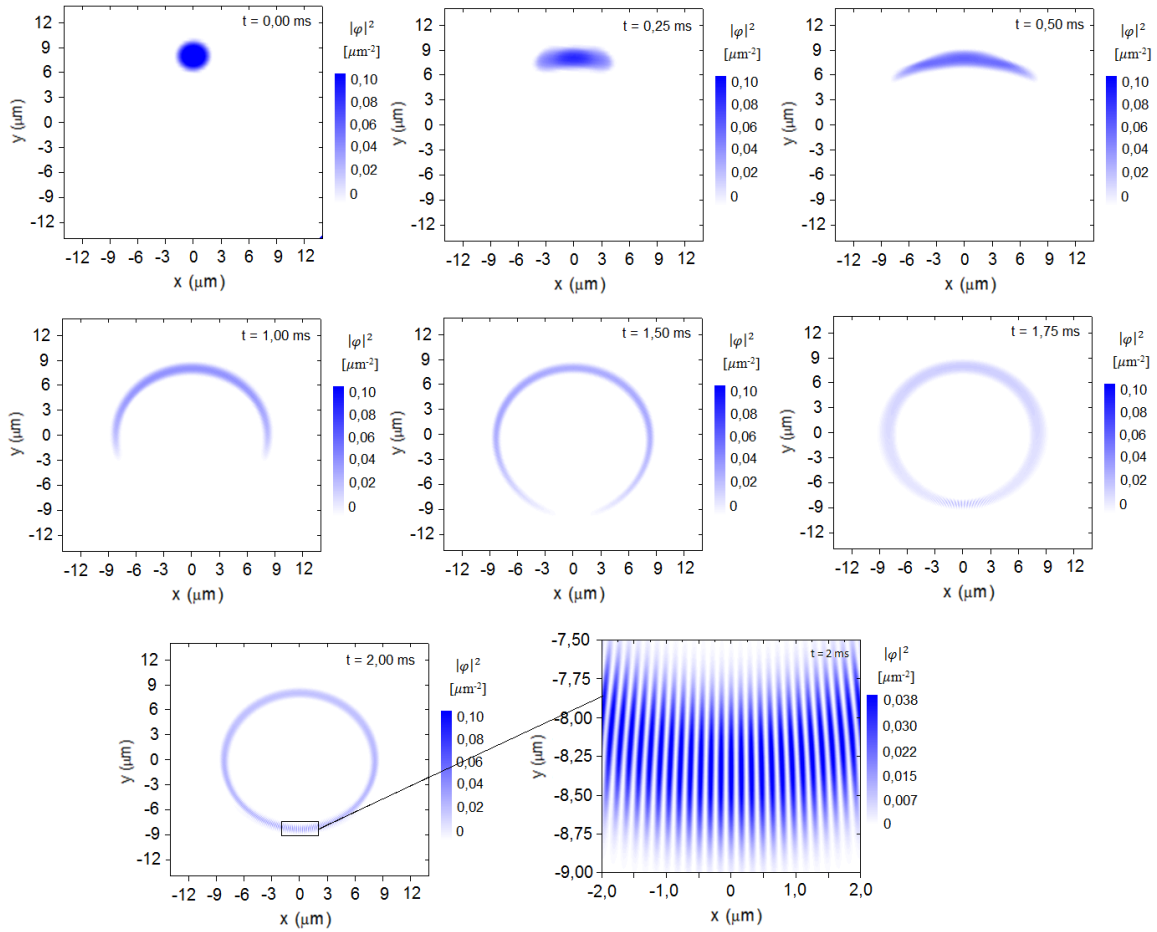

Figure 7. Density plot of the temporal evolution of the density distribution of the ^{87}Rb BEC after an initial transfer of momentum corresponding to $k = 4\ \mu\text{m}^{-1}$ in the $\pm x$ directions. Last picture shows an enlarged view of the interference region at $t = 2$ ms. The rest of parameters are the same as in Figure 3.

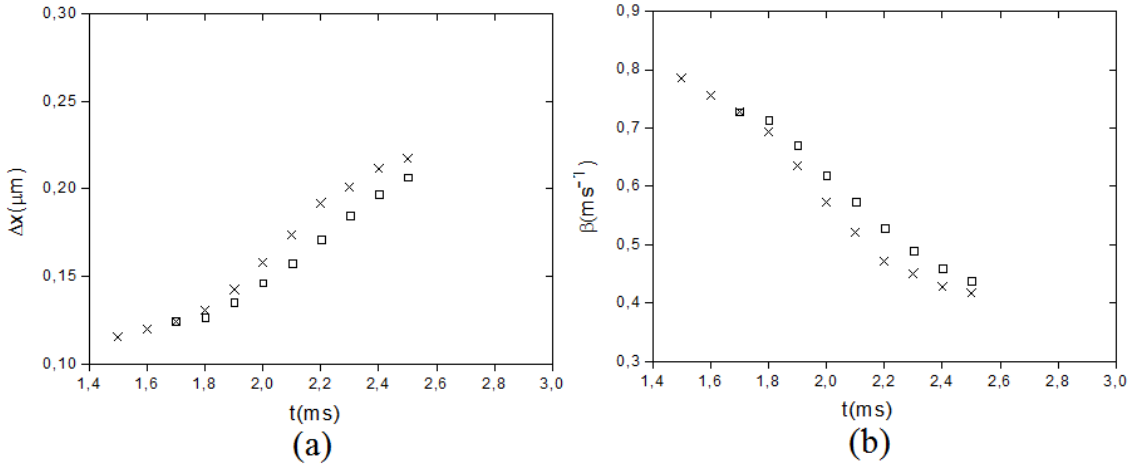

Figure 8. (a) Time evolution of the fringe spatial period for a ^{87}Rb BEC with N = 5000 atoms under free expansion (squares) and for an initial double momentum transfer of $k = 4\ \mu\text{m}^{-1}$ in opposite directions (crosses). (b) Velocity gradient $\beta(t)$ obtained from expression (12) for the free expansion case (squares) and the double momentum transfer case of $k = 4\ \mu\text{m}^{-1}$ (crosses). The rest of parameters are the same as in Figure 3.

6. Conclusions

In this work, we have numerically studied the dynamics of a ^{87}Rb BEC propagating along a 2D ring potential with the aim of exploring the possibilities that this system offers to study atomic interferences. In the third dimension, the dynamics is frozen by the presence of a strong harmonic trapping potential. The evolution of the system has been simulated by means of the Cranck-Nicholson method applied both in imaginary time for the calculation of the initial ground state and in real time for the temporal evolution. In this context, we have studied three cases: the free expansion of the repulsive condensate in the ring, the propagation after a single instantaneous transfer of momentum, and the propagation after a double instantaneous transfer of momentum in opposite directions. In all the cases, we have evaluated the fringe spatial period of the interference pattern when the BEC nearly fills completely the ring, i.e., when the clock and counter-clock wise components overlap. Finally, we have compared the numerical results with the classical approximation and calculated the velocity gradient for the nonlinear case.

7. Acknowledgements

I am grateful to my supervisors Dr. Verònica Ahufinger and Dr. Jordi Mompart for their support and collaboration in this project. I also strongly acknowledge Yu. Loiko for his support in performing the numerical simulations helping me to see how to treat the physics in them.

References

[1] M.H. Anderson *et al*., Science **269**, 198 (1995).
[2] K.B. Davis *et al.*, Phys. Rev. Lett. **75**, 3969 (1995).
[3] C.C. Bradley *et al.*, Phys. Rev. Lett. **75**, 1687 (1995).
[4] J.D. Weinstein *et al.*, Phys. Rev. A **52**, 5 (1995).
[5] R. Grimm *et al.*, Advances in atomic molecular and optical Physics, **42**, 95 (2000).
[6] K. Bongs *et al.*, Phys. Rev. A **63**, 031602(R) (2001).
[7] Maciej Lewenstein *et al.*, Advances in Physics **56**, 243 (2007).
[8] I. Lesanovsky and W. von Klitzing, Phys. Rev. Lett. **99**, 083001 (2007).
[9] A. Ramanathan *et al*., Phys. Rev. Lett., **106**, 130401 (2011).
[10] E.M. Wright, J. Arlt and K. Dholakia, Phys. Rev. A **63**, 013608 (2000).
[11] S. Franke-Arnold *et al*., Opt. Express **15**, 8619 (2007).
[12] T. Lauber *et al.*, "BEC and guided atom optics in optical micro-potentials", poster presented at Bose-Einstein Condensation 2011: Frontiers in Quantum Gases. 10 - 16 September 2011; Sant Feliu de Guixols, Spain.
[13] A. Parola *et al.*, Phys. Rev. A **72**, 063612 (2005).
[14] J. Javanainen *et al.*, Phys. Rev. A **58**, 1 (1998).
[15] Y. Lyanda-Geller *et al.*, Phys. Rev. A **61,** 043609 (2000).
[16] J. Clarke *et al., "The SQUID Handbook"* (Wiley-VCH, Weinheim, 2004).
[17] S. Richard *et al.*, Appl. Phys. B **84**, 627 (2006).
[18] T. Schulte *et al.*, Phys. Rev. A. **66**, 033602 (2002).
[19] I. Bloch *et al.*, Rev. Mod. Phys. **80**, 885 (2008).
[20] L. Pitaevskii and S. Stringari, "Bose-Einstein Condensation" (Oxford science publications, 2003).
[21] M. R. Andrews *et al.*, Science **275**, 637 (1997).